Al-Nahrain Journal for Engineering Sciences **NJES** 27(4)441-449, 2024
http://doi.org/10.29194/NJES.27040441

Preparation and Characterization of Biochar from New Precursor

Douha S. Khudair[1], Yasser I. Abdul-Aziz[2*]

Authors affiliations:
1)Department of Chemical Engineering, University of Al-Nahrain, Baghdad - Iraq.
douha.mche23@ced.nahrainuniv.edu.iq

2*) Department of Chemical Engineering, University of Al-Nahrain, Baghdad -Iraq.
yasser.i.abdulaziz@nahrainuniv.edu.iq

Paper History:

Received: 29th May 2024

Revised: 23rd Aug. 2024

Accepted: 7th Sep. 2024

Abstract

The purpose of this study is to investigate the potential of biochar derived from Peganum harmala (Pgh) seeds as an adsorbent material for wastewater treatment. Biochar is a cost-efficient, ecologically friendly, and effective bio-sorbent for a wide range of pollutants in wastewater. Researchers are investigating the production of biochar from novel biomass sources. Phosphoric acid (H_3PO_4) was utilized in a chemical activation technique to produce biochar at various concentrations (20%, 30%, and 40%). The pyrolysis process lasted three hours at 600°C in a tube furnace with an inert nitrogen gas atmosphere. Elemental analysis, Brunauer-Emmett-Teller (BET) nitrogen adsorption, scanning electron microscopy (SEM), Fourier transform infrared spectroscopy (FTIR), energy dispersive X-ray spectroscopy (EDX), The biochar was characterized using several techniques, including elemental analysis, X-ray diffraction, Fourier transform infrared spectroscopy (FTIR), Brunauer-Emmett-Teller (BET) nitrogen adsorption, scanning electron microscopy (SEM), and energy dispersive X-ray spectroscopy (EDX). The findings demonstrate the significant potential of Pgh seed-derived biochar as an inexpensive and ecologically acceptable sorbent material. A large surface area (691.58 m^2g^{-1}) was achieved at 600°C for three hours with 40% H_3PO_4 activation.

Keywords: Biochar, Peganum Harmala Seeds, Adsorption, Heavy Metal Ions, Kinetic Isotherm Models.

توليف وتوصيف الفحم الحيوي من مصادر جديدة

ضحى صباح خضير ، ياسر عماد عبد العزيز

الخلاصة:

الغرض من هذه الدراسة هو دراسة إمكانات الفحم الحيوي المشتق من بذور نبات الحرمل (Pgh) كمادة مازة لمعالجة مياه الصرف الصحي. الفحم الحيوي هو مادة مازة حيوية فعالة من حيث التكلفة وصديقة للبيئة وفعالة لمجموعة واسعة من الملوثات في مياه الصرف الصحي. يدرس الباحثون إنتاج الفحم الحيوي من مصادر جديدة للكتلة الحيوية. استُخدم حمض الفوسفوريك (H3PO4) في تقنية التنشيط الكيميائي لإنتاج الفحم الحيوي بتركيزات مختلفة (٢٠٪، ٣٠٪ و٤٠٪). استغرقت عملية الانحلال الحراري ثلاث ساعات عند درجة حرارة ٦٠٠ درجة مئوية في فرن أنبوبي مع جو خامل من غاز النيتروجين. تم توصيف الفحم الحيوي باستخدام عدة تقنيات منها تحليل العناصر، وامتصاص النيتروجين بتحويل بروناور-إيميت-تيلر(BET) ، والفحص المجهري الإلكتروني الماسح(SEM) ، والتحليل الطيفي بالأشعة تحت الحمراء بتحويل فورييه(FTIR) ، والتحليل الطيفي بالأشعة السينية المشتتة للطاقة(EDX) ، وتم توصيف الفحم الحيوي باستخدام عدة تقنيات منها التحليل العنصري وحيود الأشعة السينية والتحليل الطيفي بالأشعة تحت الحمراء بتحويل فورييه(FTIR) ، وامتصاص النيتروجين بتحويل بروناور-إيميت-تيلر(BET) ، والفحص المجهري الإلكتروني الماسح(SEM) ، والتحليل الطيفي بالأشعة السينية المشتتة للطاقة (EDX). تُظهر النتائج الإمكانات الكبيرة للفحم الحيوي المشتق من بذور الفحم النباتي كمادة مازة غير مكلفة ومقبولة بيئيًا. تم تحقيق مساحة سطحية كبيرة (٦٩١,٥٨ م٢/ جم) عند درجة حرارة ٦٠٠ درجة مئوية لمدة ثلاث ساعات مع تنشيط H3PO4 بنسبة ٤٠%. .

1.Introduction

Biochar (BC) or Several investigators are interested in activated carbon owing to its exceptional qualities, which include thermostability, high performance, strong adsorptive effect, significant surface area, and well-developed structure[1] .Wood, coal, and

NJES is an **open access Journal** with **ISSN 2521-9154** and **eISSN 2521-9162**

petroleum coke are examples of raw materials[2], that contain carbon that are converted into activated carbon via pyrolysis and activation processing[3], The material's name changes between Biochar and activated carbon depending on the raw material used , Biochar is a carbon-rich material generated from biomass (organic matter from plants) and prepared in a limited oxygen environment [4].Activated carbon, constructed from biomass or other carbonaceous materials[5]. The decrease in these resources motivates researchers to utilize natural resources from biomass as precursors for biochar[6], furthermore, One positive part of biochar production from biomass is that it can fix carbon dioxide instead of producing CO2. Another is that the biochar may be organically absorbed by soil[7].

Considering the enormous potential for raw material supply in the wood processing, carpentry, and other related industries, biochar formed from biomass waste could improve economic returns and reduce pollution. , biomasses include date stones, oil palm fiber, cotton stalks, pistachio nut shells, pomelo skin, orange peel, rice husk, pine apple peel, and mangosteen peel[8].Additionally, Biochar because of its well-developed pore structure, wide specific surface area, and abundance of surface chemical groups, it is frequently utilized as a conventional adsorbent[9], There are four different types of activated carbon i.e. Powder Activated Carbon (PAC),Granular Activated Carbon (GAC), Activated Carbon Cloth (ACC) and Activated Carbon Fibrous (ACF) depends on their shape and size [10], Carbon-rich organic compounds can be chemically or physically activated to produce activated carbon. The two steps of the physical activation process are carbonization and activation, which can be done using steam, carbon dioxide, or a mix of the two gases [11] . A chemical activation procedure involves mixing a precursor with an activating agent (H3PO4, ZnCl2, etc.) and producing activated carbon after carbonization and washing [12]. There are several benefits to the chemical activation: It is a one-step technique that works well at low temperatures, produces excellent adsorbents with mixed porosity, and has a high carbon yield [13].

2. Experimental

2.1. Materials

Biomass (peganum harmala seeds (Pgh)) sample was obtained from a community market. A biomass (peganum harmala seeds Pgh) sample was obtained from a community market. Calderoni and Mahmoudian deeply investigate Peganum harmala seeds [14-15]. The chemical components that were found by EDX analysis of Pgh are shown in Table 1, and Table 3 Chemicals used in the workplace.

Table (1): The properties of peganum harmala seeds Pgh .

Element	Atomic %	Weight %
C	58.1	49.3
O	40.1	45.3
Mg	0.3	0.4
Cl	0.2	0.5
K	0.2	0.6
Ca	0.5	1.5
Fe	0.1	0.3
Ni	0.2	0.8
Zn	0.3	1.2

2.2. Biochar preparation

In this work, a method for producing biochar (BC) using Pgh seeds as a precursor is described. The multi-step process includes, among other things, pre-treatment, activation, carbonization, and post-treatment.

2.2.1. Pre-treatment:

Using tap water and distilled water in consecutive washings eliminates dust and other foreign elements as well as any leftover impurities. Subsequently, the clean seeds are dried entirely in an electric oven at 105°C for a full day of desiccation. After that, an electric grinder is used to physically grind the dry seeds into a uniform particle size distribution of 1.18 to 1.18 mm. Sieving makes it easier to get the desired particle size fraction [16-17].

2.2.2.Activation:

The pre-treated Pgh material is impregnated during the activation stage with a phosphoric acid (H3PO4) solution. Three distinct concentrations (20%, 30%, and 40%) are used to test the influence of activation severity. A set amount of 20 grams of Pgh material is mixed with 50 millilitres of each H3PO4 solution. The impregnated samples are then dried in a water bath at 80 degrees Celsius for 24 hours. It is worth noting that the evaporation period of the surplus solution correlates positively with the concentration of H3PO4 used. Following that, any leftover moisture is removed from the samples by oven-drying them[18].

2.2.3. Carbonization

The activation phase is followed by the carbonization stage. The oven-dried and phosphoric acid-treated samples are fed into a tubular electric furnace for high-temperature processing in an inert environment. The temperature is increased at a regulated rate of 10°C/min from ambient to the goal carbonization temperature of 600°C. The samples are held at this temperature for 3 hours with a constant flow of nitrogen gas (100 cm^3/min) to prevent oxidation[18]. Following the holding period, the furnace can cool naturally before removing the biochar samples.

2.2.4. Post-treatment:

The last step involves biochar post-treatment. Deionized water is used to clean the biochar of any contaminants or reaction products left over from the activation process. This is followed by a final drying phase that uses an electric heater to eliminate any remaining moisture. The finished product is biochar that has been fully dried [19-20]. This method gives a well-defined strategy to producing biochar from Pgh seeds with flexible characteristics by changing the amount of phosphoric acid during the activation step.

Table (2): Biochar Prepared using H_3PO_4 Activation Agent.

sample	activated agent	Conc.%	Time (h)	Temp. (C)
P20	H_3PO_4	20	3	600
P30	H_3PO_4	30	3	600
P40	H_3PO_4	40	3	600

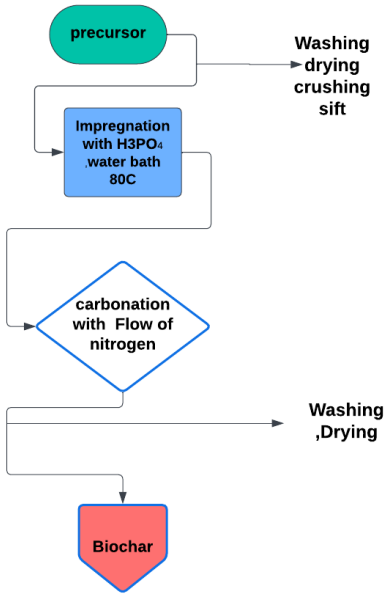

Figure (1): Schematic diagram for preparation of biochar.

Table(3): Chemicals used in the workplace

Chemicals used in the workplace	Chemical formula	Purity	The Origin
Phosphoric acid	(H_3PO_4)	85%	UK
Hydrochloric acid HCl	(HCl)	35-38%	Germany
Sodium Hydroxide	(NaOH)	97%	Germany
Ferric Chloride	($FeCl_3$)	97%	India
Nickel Chloride	($NiCl_2$)	98%	India
Lead nitrate	$Pb(NO_3)_2$	99%	India
Deionized water	H_2O	100%	Iraq

Table (4): Laboratory equipment used in the preparation stages

equipment	Description	Manufacturer
Electric oven	Maximum temperature 220 °C	Heraeus
Electric Herb Grain Grinder	Power rate: 220 Volts, Frequency: 50 Hz	silver crest
Hot plate magnetic stirrers	Speed: 60-1500 rpm, Maximum temperature: +380°C	Labteach
Tubular electric furnace	Max. Working Temperature1650C	Aady Group
Electronic Balance	Maximum weight 220g , Minimum weight 0.0001g	Sartorius

3. Investigate the characteristics of biochar.

Table (5): Laboratory measuring and testing equipment used in the work

Testing device	Description	Manufacturer
X-ray diffraction (XRD)	Nondestructive method that offers comprehensive details on the crystal structure.	Panalytical
Energy Dispersive X-Ray Spectroscopy (EDX)	method for determining a material's elemental composition.	HRSEM
Brunauer, Emmett,and Teller (BET)surface area analysis	a measure of the exposed surface of a solid sample on the molecular scale	HORIBA Scientific
Fourier Transform Infrared Spectroscopy (FTIR)	identifies a molecule's chemical bonds by generating an infrared absorption spectra.	Bruker Alpha
Scanning electron microscopy (SEM)	The instrument is able to generate high-resolution images, measuring with deep accuracy infinitesimal aspects of organic and inorganic objects	Thermo Fisher Scientific
Thermo Gravimetric Analysis (TGA)	a powerful technique for the measurement of thermal stability of materials including polymers	TA Instruments
Atomic Absorption spectrometry (AAS)	measures the concentration of specific elements in a sample	analytik jena

Table (6): Properties of Peganum harmala seeds (Pgh) and biochar.

Element	**Weight % Pgh**	**Weight % Biochar**
C	49.3	63.1
O	45.3	19.1
Mg	0.4	0
Cl	0.5	0
K	0.6	0
Ca	1.5	0.3
Fe	0.3	0.4
Ni	0.8	1
Zn	1.2	0
N	0	4.6
Na	0	0.6
P	0	10.8

3.1. Surface Area of AC

The Surface Area Analyzer apparatus, model SA-9600 Qsurf series by Thermo Electron Corporation using the BET test technique, was used to measure the surface area of the Biochar generated.

3.2. XRD analysis

The identity of optimum activated carbon prepared was tested using an Panalytical X-ray Diffractometer, equipped with Cu Kα radiation, λ = 0.154 nm), with a step size of 0.05° in the 2 θ range from 10 to 80° (high angle) and fixed power source 45Kv, 30mA.

3.3. EDX analysis

The chemical composition was determined through Energy Dispersive X-ray Spectroscopy (EDX), which is carried out using Thermo Scientific Axia ChemiSEM, US.

3.4. SEM analysis

Analyzed the microstructures and surface morphology of the Biochar using a scanning electron microscope (HRSEM FEI Inspect F50, USA).

3.5. FTIR analysis

FTIR Spectroscopy, Fourier-transform infrared spectroscopy, is concerned with the vibration of molecules. Each functional group has its own discrete vibrational energy which can be used to identify a molecule through the combination of all of the functional groups. (FTIR) was done in (Bruker Alpha/ USA). The spectra recorded the result from 4000 to 400 cm-1 resolution in the mid-infrared region.

3.6. Pore structure of activated carbons

Extraction of porosity and pore size distribution from SEM images using MATLAB programmer. It's assume that the input SEM images are gray-scale and darker parts of the image shows deeper surfaces which are considered as pore spaces.

3.7. Thermo Gravimetric Analysis (TGA)

Tested with a weight of 9.946 gm pgh sample at a temperature rising rate of 20 °C/min up to 930 °C in the N_2 atmosphere. The device used in the test is (SDT Q600 V20.9 Build 20, Module DSC-TGA Standard) Temperature range: 44.40 to 980.24 °C .

4. Result and Discussion

4.1. Surface Area of AC

The maximum surface area achieved in the study was 691.58 m2/g with a 40% H_3PO_4 concentration at an activation temperature of 600°C for 3 hours [21]. Increased levels of phosphorous compounds reacting with lignocellulosic materials during impregnation and activation stages could lead to this issue.[22].

Table (7): surface area of biochar.

label	Chemical method	method Conc. (%)	Surface area (BET) m^2 /g
Pgh	-	-	0.128
P20	H_3PO_4	20	322.98
P30	H_3PO_4	30	554.09
P40	H_3PO_4	40	691.58

4.2. X-ray Diffraction (XRD) Analysis of Biochar Crystallinity

Adsorption and Crystallinity: The importance of determining an adsorbent material's crystallinity is emphasized in this section in order to get the best possible adsorption results. Powder X-ray diffraction (XRD) is an essential instrument for:

1. Measuring Crystalline Content: Figuring out how much crystalline material is in the adsorbent.
2. Determining Crystalline Phases: Describe the particular kinds of crystalline formations that are there.
3. Lattice plane spacing is the measurement of the separation between atomic planes in a crystal lattice [23].X-ray Diffraction Analysis of Biochar The methods used to analyze the biochar samples with an XRD device (XRD-6000, Shimadzu) are described. Significant variables consist of: Cu Kα radiation with a wavelength (λ) of 1.5406 Å is the source of radiation. Operating conditions: Continuous scan mode at 40 kV and 30 mA. Range of Scan: 2θ = 10°–80°.1° per minute is the scan rate. Analysis of X-ray diagrams: Examining the P_{40} biochar sample Figure (2 indicates that three wide diffraction peaks are present at different 2θ locations.2θ = 10°–30°: Denotes a chaotic arrangement of stacked carbon rings and the existence of amorphous carbon.

Peaks and Crystalline Structure Correspondence: The observed peaks are further analyzed based on known literature: Amorphous carbon may occur, as shown by the peak at 2θ = 25 [24].

Peaks at 2θ = 44°: Associated with the formation of pores as a result of carbon breaking down along the graphitic structures' direction[13].Peak at 79°: Maybe a sign of tiny organized graphene sheet domains inside the activated carbon [25].To sum up, the XRD study offers important new information on the crystalline structure of the biochar made from Peganum harmala seeds. The structural properties of the biochar are highlighted by the observed amorphous carbon and the possible presence of ordered graphene domains, which can substantially impact the biochar's ability to adsorb materials for use in wastewater treatment applications.

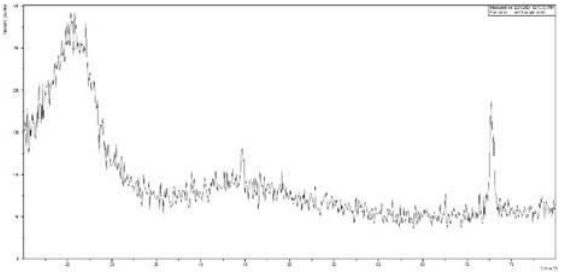

Figure (2): XRD for the prepared Biochar.

4.3. EDX analysis of the prepared biochar

Figure 3 and table 8 display the EDX assessment test results, indicating the percentage of elemental composition values of the raw material and the biochar.

The carbon content of precursors increased from 49.3% to 63.1% after undergoing carbonization and activation processes. Carbon levels rise as heat causes decomposition in the carbonization process, eliminating non-carbon and volatile components and converting them into carbon. The ash content of biochar is 17.7%. Ash content is the residual mineral material left behind after combustion.

Table (8): EDX Analysis of the prepared biochar

Element	Atomic %	Atomic % Error	Weight %	Weight % Error
C	73.1	0.6	63.1	0.5
N	4.5	1.2	4.6	1.2
O	16.7	0.6	19.1	0.7
Na	0.4	0.0	0.6	0.1
P	4.8	0.1	10.8	0.1
Ca	0.1	0.0	0.3	0.1
Fe	0.1	0.0	0.4	0.1
Ni	0.2	0.0	1.0	0.2

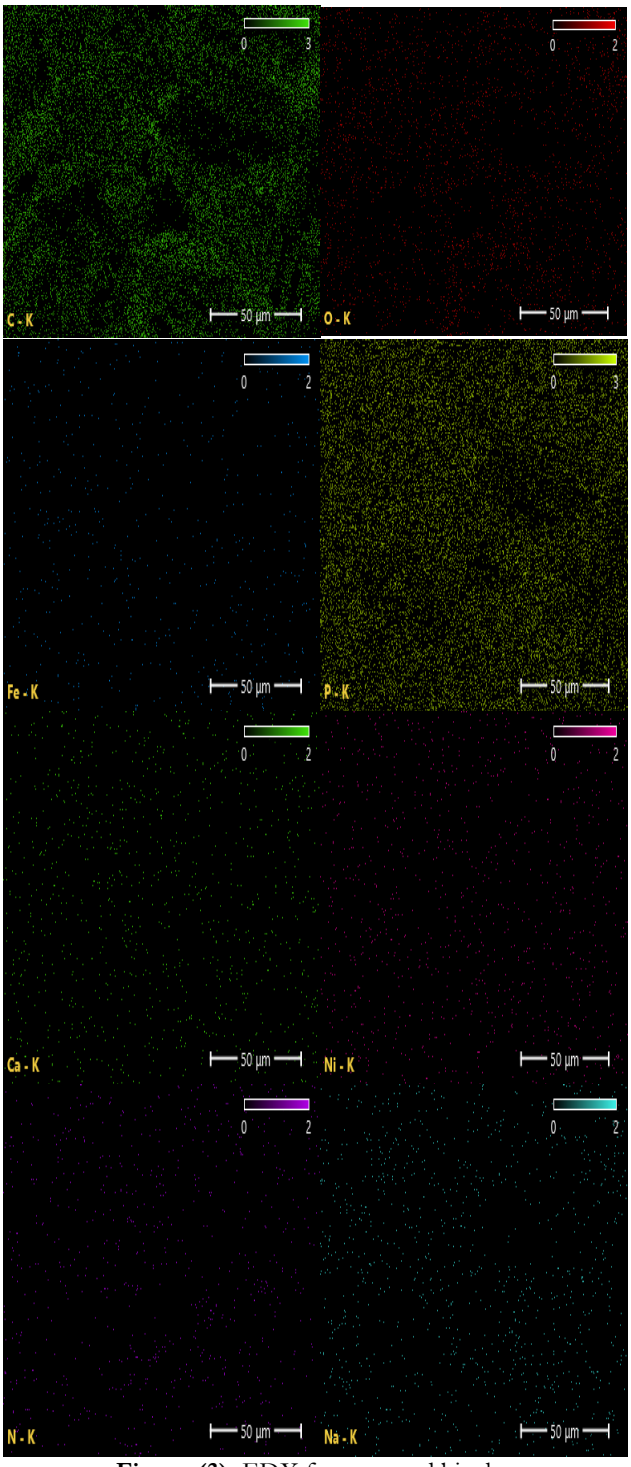

Figure (3): EDX for prepared biochar.

4.4. SEM analysis for the prepared biochar

The surface physical morphology of the material was observed using the SEM method. The scanning electron microscope (SEM) pictures displayed the porous structure of Pgh and Pgh-derived biochar, as shows in Figure (a and b). The results indicated that the activated carbon formed an unequal, highly porous surface with open, uniform macropores on the outer surfaces. The biochar showed a well-developed pore structure. The formation of micropores during carbonization is important for the adsorption of heavy metals since it improves the surface area available for absorption. The H_3PO_4 impregnation with the precursor likely caused the breakdown of lignin and hemicellulose, leading to a reduction in cellulose crystallinity and the formation of high porosity.

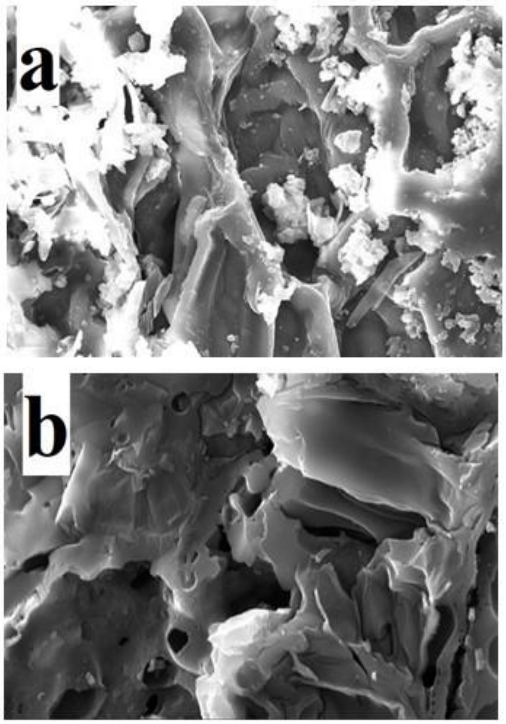

Figure (4): Scanning electron microscopy (SEM):(a) Peganum harmala seeds before activation (b) Peganum harmala seeds after activation.

4.5. FTIR Analysis

This section uses FTIR spectroscopy to investigate the functional group makeup of the Pgh precursor and the biochar that was generated from it.

FTIR analysis of the Pgh precursor revealed the following important functional groups, which corresponded to different wavenumbers[26]:

- O-H stretching: Shows that hydroxyl (-OH) groups are present. It is centered at 3272.59 cm^{-1} and spans 3000–3500 cm^{-1}.
- The alkyl C-H stretching (2922.78 cm^{-1}) indicates the possible existence of chains of aliphatic hydrocarbons.
- Aryl-substituted C=C stretching (1624.33 cm^{-3}): This suggests that aromatic rings are present.
- The stretching of alkyl carbonate (1743.02 cm^{-1}) indicates the presence of ester groups.
- C-O stretching (1199.16 cm^{-1}): Denotes the existence of a variety of functional groups

involving C-O bonds, including acids, alcohols, phenols, ethers, and/or esters.

- **FTIR Analysis of Biochar**

When the biochar is analyzed, it shows a different functional group profile from the Pgh precursor. The following functional groupings were determined to be possible [[27],[28]]:

- Aromatic rings or unsaturation (C=C-H) (3080.37 cm^{-3}).
- C≡C stretch (2124.05 cm^{-1}) in terminal alkynes (monosubstituted compounds).
- Aryl disulfides' S-S stretch is 453.14 cm^{-3}.
- Secondary amines with a CN stretch (1176.03 cm^{-1}).
- Stretch of carboxylate (sodium carboxylic acid) (1550.02 cm^{-3}).
- C-H aromatic (752.34 cm^{-1}).

Comparing the Function Groups:

There is a noticeable change in the functional groups between the biochar and the Pgh precursor[29]:

- Hydroxyl (-OH) Groups: These groups vanish in the biochar, indicating that pyrolysis removed them.
- Unsaturated Compounds: During pyrolysis, these compounds break and transform into volatile gas or liquid products, which causes them to disappear.
- Aliphatic C-H: At higher temperatures, these bonds break, which causes them to vanish from the biochar.
- Aromatic Rings: At high pyrolysis temperatures, rearrangement causes the aromatic rings' structure to deteriorate.
- Novel Functional Groups: The biochar shows the presence of functional groups such C ≡ C in terminal alkynes, aryl disulfides, and secondary amines that were not present in the precursor.
- Carboxylate Groups: The Pgh precursor and the biochar both include these groups.

Effect of Heat on Functional Groups:

The text highlights the impact of temperature on different functional groups during pyrolysis. It explains that weight loss occurs before cellulose reaches 300°C[30], and water molecules are released at 200°C. Gaseous hydrocarbon formation occurs at temperatures between 400°C and 500°C[10], reducing hydrogen content. FTIR spectroscopy reveals significant differences in the functional group profile of biochar compared to the Pgh precursor. This is due to the removal of hydroxyl groups, transformation of unsaturated molecules, and formation of new functional groups, which could significantly affect biochar's adsorption capabilities for wastewater treatment.

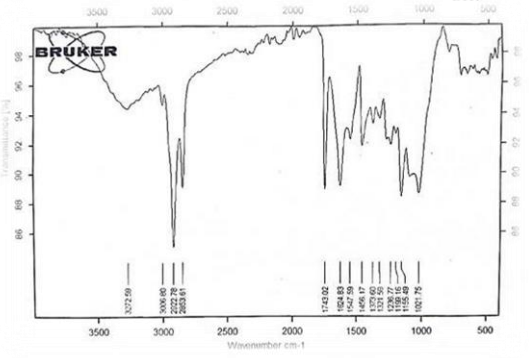

Figure (5): FTIR spectra of raw material.

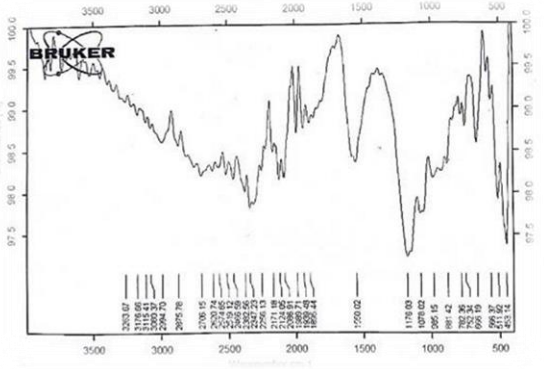

Figure (6): FTIR spectra of activated carbon prepared.

4.6. Pore structure of biochar

In recent years, a unique approach for characterizing materials has emerged: employing image processing tools to study the structure of material data captured in SEM images. Andrzej and his coworker [31] recommended utilizing SEM image analysis software to evaluate membrane porosity. Using digital image technologies and the box number dimensions technique, Zou and his workmate [32]examined coal sample porosity and fractal size. Digital image processing was used by Cardell and his co-workers [33] using backscattered electron (BSE) images and X-ray elemental maps to quantify and ascertain the depth of the porous salt medium and porosity.[34] present a method for exploiting scanning electron microscopy (SEM) images to estimate the pore size distribution of porous materials. A Visual Basic program was created to put the strategy to the test. To split the image into bright and dark regions, which were assumed to be pores, a threshold value was set. The threshold value may be determined using the cumulative frequency of the image's pixel intensities. This study use MATLAB software image analysis to evaluate the pore size statistics characterization technique of disordered mesoporous materials using SEM pictures. The MATLAB program runs and produces five outputs in the main file: four distinct photos and a composite image summarizing the analysis (similar to the supplied example).

Individual Images:

Individual photos:

- Four high-resolution SEM photos (Fig. 7) show the porous material at different magnification levels. SEM photograph surfaces with a focused electron beam, implying that these pictures share

a similar origin. The dark patches in the micrographs show holes in the material.

- The second image shows a depth map with colored pixel clusters. Variations in pixel intensity are presumably related to surface elevation, with brighter and darker pixels perhaps representing greater and lower altitudes, respectively.
- The third image displays a binary segmentation image. Each pixel is classed as pore space (white) or backdrop (black).
- The fourth figure shows a pore size distribution graph. This graph shows the link between pore radius (μm) on the x-axis and frequency (y-axis). The observed histogram reveals a preponderance of smaller pores over bigger ones.

Porosity Calculation:

The algorithm determines the material's porosity, which in this case is 0.27029. Porosity is a material attribute that describes the amount of empty space within it. In this research, pore space refers to the material's unoccupied spaces.

Data Validation:

For validation, the computer does a comparison study of numerous photos. This approach produces findings with a high degree of similarity, indicating consistent and trustworthy picture processing.

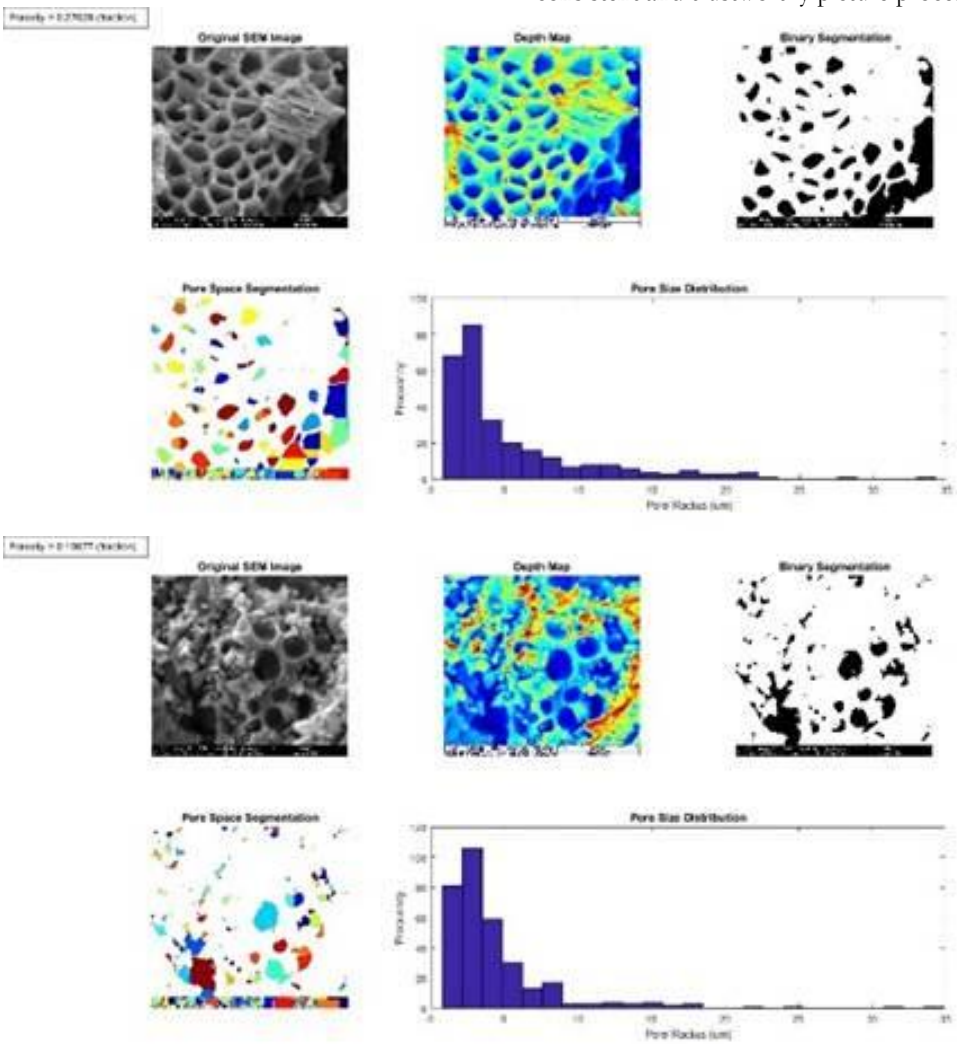

Figure (7): Pore structure of biochar

4.7. Thermo Gravimetric Analysis (TGA)

Figure (8 showing the change in weight of a Peganum harmala seeds (Pgh) sample as a function of temperature.

Observations of TGA:

The linear mass decrease tendency shown in the TGA curve suggests that weight is continuously lost as the temperature increases from 0°C to 1000°C. It can seen a first weight loss at 100 °C, which is the beginning of thermal breakdown when volatile chemicals from the Pgh sample are released. The main devolatilization stage is corresponding to the substantial mass loss between 100°C and 500°C. This implies that important Pgh components have broken down. finally slow loss in mass continues up to 900 °C. The Pgh sample had a total mass loss of 90.33%, which Balasundram [35] corroborate, maybe because of its high volatile matter concentration.

These are the anticipated phases of pyrolytic breakdown [36]**.**

- Elimination of moisture usually happens below 220 °C in a pyrolysis setting (without oxygen).
- It is between 220°C and 315°C when hemicellulose breaks down.
- Decomposition of cellulose takes place between 315 and 400 °C.

- At temperatures higher than 400 °C, lignin breakdown takes front stage.

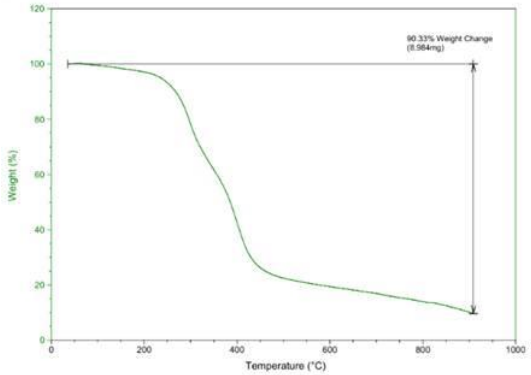

Figure (8): Thermogravimetric Analysis (TGA) of the Components of peganum harmala seeds.

5. References:

[1] J. Andas, M. L. A. Rahman, and M. S. M. Yahya, "Preparation and Characterization of Activated Carbon from Palm Kernel Shell," in *IOP Conference Series: Materials Science and Engineering*, Institute of Physics Publishing, Aug. 2017. doi: 10.1088/1757-899X/226/1/012156.

[2] M. Iwanow, T. Gärtner, V. Sieber, and B. König, "Activated carbon as catalyst support: Precursors, preparation, modification and characterization," *Beilstein Journal of Organic Chemistry*, vol. 16. Beilstein-Institut Zur Forderung der Chemischen Wissenschaften, pp. 1188–1202, Jun. 02, 2020. doi: 10.3762/bjoc.16.104.

[3] Y. R. Abdulmajeed, N. Al-Huda, and J. Mahmood, "Production of High Surface Area Activated Carbon from Grass (Imperata)," *Iraqi Journal of Chemical and Petroleum Engineering*, vol. 19, no. 2, pp. 33–37, 2018, [Online]. Available: www.iasj.net

[4] X. , L. S. , L. Y. , G. Y. , Z. G. , H. X. , W. X. , L. S. , & J. L. Tan, "Biochar as potential sustainable precursors for activated carbon production: Multiple applications in environmental protection and energy storage," vol. 227, pp. 359–372, May 2017, doi: https://doi.org/10.1016/j.biortech.2016.12.083.

[5] N. Hagemann, K. Spokas, H. P. Schmidt, R. Kägi, M. A. Böhler, and T. D. Bucheli, "Activated carbon, biochar and charcoal: Linkages and synergies across pyrogenic carbon's ABCs," *Water (Switzerland)*, vol. 10, no. 2. MDPI AG, Feb. 09, 2018. doi: 10.3390/w10020182.

[6] H. Tounsadi, A. Khalidi, M. Abdennouri, and N. Barka, "Activated carbon from Diplotaxis Harra biomass: Optimization of preparation conditions and heavy metal removal," *J Taiwan Inst Chem Eng*, vol. 59, pp. 348–358, Feb. 2016, doi: 10.1016/j.jtice.2015.08.014.

[7] M. S. Reza *et al.*, "Preparation of activated carbon from biomass and its' applications in water and gas purification, a review," *Arab Journal of Basic and Applied Sciences*, vol. 27, no. 1. Taylor and Francis Ltd., pp. 208–238, Jan. 01, 2020. doi: 10.1080/25765299.2020.1766799.

[8] M. J. Ahmed and S. K. Theydan, "Adsorption of cephalexin onto activated carbons from Albizia lebbeck seed pods by microwave-induced KOH and K2CO3 activations," *Chemical Engineering Journal*, vol. 211–212, pp. 200–207, Nov. 2012, doi: 10.1016/j.cej.2012.09.089.

[9] J. Li *et al.*, "Comparative Study on the Adsorption Characteristics of Heavy Metal Ions by Activated Carbon and Selected Natural Adsorbents," *Sustainability (Switzerland)*, vol. 14, no. 23, Dec. 2022, doi: 10.3390/su142315579.

[10] N. K. Gupta, P. Prakash, P. Kalaichelvi, and K. N. Sheeba, "The effect of temperature and hemicellulose-lignin, cellulose-lignin, and cellulose-hemicellulose on char yield from the slow pyrolysis of rice husk," *Energy Sources, Part A: Recovery, Utilization and Environmental Effects*, vol. 38, no. 10, pp. 1428–1434, May 2016, doi: 10.1080/15567036.2014.941518.

[11] M. Boshir Ahmed, M. Abu Hasan Johir, J. L. Zhou, H. Hao Ngo, L. D. Nghiem, and H. Johir, "Activated carbon preparation from biomass feedstock: Clean production and carbon dioxide adsorption," *Journal of Cleaner Production* , vol. 225, pp. 405–413, 2019, doi: DOI:10.1016/j.jclepro.2019.03.342.

[12] D. Das, D. P. Samal, and M. BC, "Preparation of Activated Carbon from Green Coconut Shell and its Characterization," *Journal of Chemical Engineering & Process Technology*, vol. 06, no. 05, 2015, doi: 10.4172/2157-7048.1000248.

[13] Y. Elmaguana, N. Elhadiri, M. Bouchdoug, M. Benchanaa, and A. Jaouad, "Optimization of preparation conditions of activated carbon from walnut cake using response surface methodology," 2018. [Online]. Available: http://revues.imist.ma/?journal=morjchem&page=login

[14] M. Calderoni, M. Altare, L. Mastracci, F. Grillo, L. Cornara, and A. Pagano, "Potential risks of plant constituents in dietary supplements: Qualitative and quantitative analysis of Peganum harmala seeds," *Molecules*, vol. 26, no. 5, 2021, doi: 10.3390/molecules26051368.

[15] M. Mahmoudian, H. Jalilpour, and P. Salehian, "Toxicity of Peganum harmala: Review and a Case Report," 2002. [Online]. Available: http://ijpt.iums.ac.ir

[16] E. Köseoğlu and C. Akmil-Başar, "Preparation, structural evaluation and adsorptive properties of activated carbon from agricultural waste biomass," *Advanced Powder Technology*, vol. 26, no. 3, pp. 811–818, May 2015, doi: 10.1016/j.apt.2015.02.006.

[17] M. Ullah *et al.*, "The effective removal of heavy metals from water by activated carbon adsorbents of Albizia lebbeck and Melia azedarach seed shells," *Soil and Water Research*, vol. 15, no. 1, pp. 30–37, 2020, doi: 10.17221/212/2018-SWR.

[18] M. M. N. Aljumaili and Y. I. Abdul-Aziz, "High surface area peat moss biochar and its potential for Chromium metal adsorption from aqueous solutions," *S Afr J Chem Eng*, vol. 46, pp. 22–34, Oct. 2023, doi: 10.1016/j.sajce.2023.06.006.

[19] S. Timur, I. C. Kantarli, S. Onenc, and J. Yanik, "Characterization and application of activated carbon produced from oak cups pulp," *J Anal Appl Pyrolysis*, vol. 89, no. 1, pp. 129–136, 2010, doi: 10.1016/j.jaap.2010.07.002.

[20] T. Tay, S. Ucar, and S. Karagöz, "Preparation and characterization of activated carbon from waste biomass," *J Hazard Mater*, vol. 165, no. 1–3, pp. 481–485, Jun. 2009, doi: 10.1016/j.jhazmat.2008.10.011.

[21] T. Khadiran, M. Z. Hussein, Z. Zainal, and R. Rusli, "Textural and Chemical Properties of Activated Carbon Prepared from Tropical Peat Soil by Chemical Activation Method," 2015.

[22] S. M. Yakout and G. Sharaf El-Deen, "Characterization of activated carbon prepared by phosphoric acid activation of olive stones," *Arabian Journal of Chemistry*, vol. 9, pp. S1155–S1162, Nov. 2016, doi: 10.1016/j.arabjc.2011.12.002.

[23] S. Afroze and T. K. Sen, "A Review on Heavy Metal Ions and Dye Adsorption from Water by Agricultural Solid Waste Adsorbents," *Water Air Soil Pollut*, vol. 229, no. 7, Jul. 2018, doi: 10.1007/s11270-018-3869-z.

[24] Y. H. Chiu and L. Y. Lin, "Effect of activating agents for producing activated carbon using a facile one-step synthesis with waste coffee grounds for symmetric supercapacitors," *J Taiwan Inst Chem Eng*, vol. 101, pp. 177–185, Aug. 2019, doi: 10.1016/j.jtice.2019.04.050.

[25] and S. H. Qu Deyang, "Studies of the activated carbons used in double-layer supercapacitors," *J Power Sources*, vol. 109, no. 2, pp. 403–411, Jul. 2002, doi: 10.1016/S0378-7753(02)00108-8.

[26] A. B. D. Nandiyanto, R. Oktiani, and R. Ragadhita, "How to read and interpret ftir spectroscope of organic material," *Indonesian Journal of Science and Technology*, vol. 4, no. 1, pp. 97–118, 2019, doi: 10.17509/ijost.v4i1.15806.

[27] J. Coates, "Interpretation of Infrared Spectra, A Practical Approach."

[28] Y. E. Lee, J. H. Jo, I. T. Kim, and Y. S. Yoo, "Chemical characteristics and NaCl component behavior of biochar derived from the salty food waste by water flushing," *Energies (Basel)*, vol. 10, no. 10, Oct. 2017, doi: 10.3390/en10101555.

[29] R. Xiao and W. Yang, "Influence of temperature on organic structure of biomass pyrolysis products," *Renew Energy*, vol. 50, pp. 136–141, Feb. 2013, doi: 10.1016/j.renene.2012.06.028.

[30] H. Yang, R. Yan, H. Chen, D. H. Lee, and C. Zheng, "Characteristics of hemicellulose, cellulose and lignin pyrolysis," *Fuel*, vol. 86, no. 12–13, pp. 1781–1788, Aug. 2007, doi: 10.1016/j.fuel.2006.12.013.

[31] T. Mao, Q. Su, and Y. Cheng, "Statistical method of pore size distribution of disordered mesoporous materials based on electron microscope imaging," in *Journal of Physics: Conference Series*, Institute of Physics, 2022. doi: 10.1088/1742-6596/2321/1/012008.

[32] G. Zou, J. She, S. Peng, Q. Yin, H. Liu, and Y. Che, "Two-dimensional SEM image-based analysis of coal porosity and its pore structure," *Int J Coal Sci Technol*, vol. 7, no. 2, pp. 350–361, Jun. 2020, doi: 10.1007/s40789-020-00301-8.

[33] C. Cardell, A. Yebra, and R. E. Van Grieken, "Applying Digital Image Processing to SEM-EDX and BSE Images to Determine and Quantify Porosity and Salts with Depth in Porous Media," 2002.

[34] Abdullah et al., *A Method to Measure Pore Size Distribution of Porous Materials Using Scanning Electron Microscopy Images*. American Institute of Physics, 2010. doi: DOI:10.1063/1.3515554.

[35] V. Balasundram *et al.*, "Thermal Characterization of Malaysian Biomass via Thermogravimetric Analysis," 2018. [Online]. Available: https://jest.utm.my/index.php/jest

[36] M. J. Serapiglia, K. D. Cameron, A. J. Stipanovic, and L. B. Smart, "Analysis of biomass composition using high-resolution thermogravimetric analysis and percent bark content for the selection of shrub willow bioenergy crop varieties," *Bioenergy Res*, vol. 2, no. 1–2, pp. 1–9, Jun. 2009, doi: 10.1007/s12155-008-9028-4.